Coordinated Adaptive Impedance Control of Redundantly Actuated Parallel Manipulators

Journal:	*IEEE Transactions on Human-Machine Systems*
Manuscript ID	THMS-23-08-0340
Manuscript Type:	Regular Paper (S1)
Date Submitted by the Author:	08-Aug-2023
Complete List of Authors:	Ma, Nan; Lancaster University, Engineering Cheneler, David; Lancaster University, Department of Engineering He, Guangping; North China University of Technology, Mechanical and Electrical Engineering Yuan, Junjie; North China University of Technology, Department of Mechanical and Electrical Engineering Bian, Gui-Bin; Chinese Academy of Sciences, State Key Laboratory of Management and Control for Complex Systems
Keywords:	Robotics, Safety, Adaptive Systems, Assistive Robots, Bio-inspired Systems
Note: The following files were submitted by the author for peer review, but cannot be converted to PDF. You must view these files (e.g. movies) online.	
Experiment Video 1.mp4 Experiment Video 2.mp4	

Coordinated Adaptive Impedance Control of Redundantly Actuated Parallel Manipulators

Nan Ma, David Cheneler, Guangping He, Junjie Yuan and Gui-Bin Bian

***Abstract*—Redundantly actuated parallel mechanisms (RAPM) have been widely adopted in advanced robotic systems and precision machine tools. It has been demonstrated that redundant actuation can improve the performance of mechatronic systems but introduce challenges with respect to control. One main difficulty is in establishing an accurate dynamic model of the RAPM system. With an inaccurate dynamic model, the torque applied by the actuators will be incorrect, leading to increased antagonistic forces in the system. To solve this problem, a novel coordinated adaptive impedance control (CAIC) approach based on a new adaptive impedance control (AIC) law is presented here, along with proof of the stability of the closed-loop system. The control algorithm has been validated experimentally by a prototype cable-driven parallel manipulator. It can be seen from the experimental results that the proposed control method is an effective way to correct the antagonistic forces of the system, thus facilitating the improvement of its dynamic performance and its efficacy in different applications.**

***Index Terms*—Adaptive impedance control, Coordination control, Actuation redundancy, Parallel manipulators, Uncertain model**

I. Introduction

RAPMs are widely used in modern precision machine tools [1], high-speed parallel manipulators [2], musculoskeletal robots [3]-[7] and robot-aided rehabilitation training [8]-[11]. RAPMs are usually divided into two categories: parallel mechanisms with redundant drive branch chains [12], [13], i.e., with one or more branch chains with independent actuators added to a fully-driven parallel mechanism; and parallel mechanisms with redundant driving joints [14], i.e., with actuators added to one or more passive joints in a fully-driven parallel mechanism. Since the number of independent actuators is higher than the number of kinematic degrees of freedom (DOF) of a RAPM, forces can be controlled more flexibly. The redundant actuation can therefore prevent singular forces with the following advantages: 1) the operational space of the parallel mechanism can be expanded; 2) the load capacity of the manipulators can be increased by homogenizing the actuator's output; 3) the structural stiffness of the parallel mechanism can be adjusted by controlling the antagonistic forces/torques; 4) the transmission clearances of the mechanism can be minimized [15].

The main challenge for operating RAPMs is in the development of its control system. When the kinematic model of a RAPM is inaccurate, the antagonistic forces/torques in the RAPM generated by current model-based control methods can be excessively large and unbalanced [12]-[15], leading to the overload of the actuators and loss of accuracy in the transmission system. To solve this problem, a tailor-made robust control scheme was proposed by Müller [12], but this control scheme did not consider applications of the RAPM with physical interactions. However, the RAPM has been widely used in humanoid robots [3], rehabilitation robots [8]-[11], [16]-[18], exoskeleton robots [3]-[7],[19]-[20], surgical robots [21], and continuum robots [22], as well as in industrial applications, where adjusting or controlling the dynamic characteristics of the robots to accommodate physical interactions during operation is critical to achieve accuracy and safety [1],[2],[15],[22].

To attempt to equip a robot system with the afore mentioned characteristics, impedance control has been adopted by many researchers [4],[6],[8]-[26]. Recently, this was extended by use of variable impedance control [6],[16],[22],[27]-[33] to improve the adaptability of the robot system for coping with operations that change over time. This enabled the improvement of the performance of human-robot physical interaction (HRPI) systems by adjusting their inertia, stiffness and damping as required. Heretofore, due to the challenges of designing time-varying closed-loop systems, the stability region of these systems was determined experimentally [16],[27]-[29]. The approaches for the stability analysis of variable impedance control systems can be divided into two categories: energy tank-based methods [32], which are dependent on the state of the system and cannot be used for off-line design of the time-varying impedance control system as required to ensure uniform globally asymptotic stability; and stability analysis methods that use the adaptive control system as the reference, where the obtained stability conditions are not dependent on the system's state [22],[30],[33]. However, the second method assumes that the expected inertial matrix of the closed-loop system is constant. This is the main limitation since this assumption is inconsistent with the characteristics of many practical systems.

To overcome the practical difficulties of establishing accurate models of robot systems, AIC [8]-[10],[17]-[21], [34]-[36], robust AIC [37]-[40], impedance learning [41]-[49],

This work was supported in part by the National Key R&D Program of China under Grant No. 2019YFB1309603; National Natural Science Foundation of China under Grant No. 51775002; Beijing Natural Science Foundation under Grant No. KZ202010009015. *(Corresponding author: Guangping He)*

N. Ma (Corresponding author, e-mail: nan.ma401@gmail.com) and David Cheneler (d.cheneler@lancaster.ac.uk) are with the School of Engineering, Lancaster University, Lancaster, LA1 4YW, United Kingdom.

G. He (e-mail: hegp55@ncut.edu.cn), J. Yuan (e-mail: yuanjj@ncut.edu.cn) are with the Department of Mechanical and Electrical Engineering, North China University of Technology, Beijing, Jin Yuan Zhuang Road No.5, 100144, P.R. China.

G-B. Bian(guibin.bian@ia.ac.cn) is with the State Key Laboratory of Management and Control for Complex Systems, Institute of Automation, Chinese Academy of Science, 95 Zhongguancun East Road, Haidian, Beijing 100190, China.

model predictive impedance control [50], and other related control methods [51]-[57] have been studied in recent years. Most of the AIC methods developed previously are based on the framework of the conventional model reference adaptive control (MRAC) method. It is well known that the MRAC method requires a complete nonlinear dynamic model to construct the key nonlinear structure: that is, the *regressor*. When the nonlinear terms of an uncertain dynamic system are hard to fully express, the regressor constructed by the traditional MRAC method will deviate from the dynamic behavior of the actual system. This will not only lead to the deterioration of the efficacy of the closed-loop system, but also result in the corresponding non-adaptive *asymptotic* controller not necessarily stabilizing [58]. To overcome the issues with using the linear parameterization assumption often made when using the conventional MRAC method, some researchers have used neural networks [34],[56], support vector machines, Gaussian mixture models and reinforcement learning [49] methods to generate the nonlinear dynamic model of robotic systems online. This class of MRAC method can generally provide uniformly ultimately bounded (UUB) stability.

Since the main application of impedance controlled robotic systems is for interactive operations, the optimal impedance adaptive control [51] and the unified motion/force/impedance control [57] methods have also been studied with consideration of the uncertainty of the environment. The optimal impedance adaptive control method proposed in [51] was established based on the output feedback adaptive dynamic programming method. The unified motion/force impedance control method proposed in [57] uses the recursive least squares law to estimate the environmental characteristic parameters and determine the dynamic trajectory adaptation based on solving the constrained optimization problem online. Since these methods need completely online iterative optimization, they are difficult to apply to the real-time control of the multi DOFs robot systems.

Besides interactions with the environment generally, AIC has also been studied to improve the performance of HRPI systems, such as haptic interfaces [41], exoskeleton robots [4]-[7], [19]-[20] and rehabilitation robot systems [8]-[11]. In these applications, the environment faced by the robot system includes a part of the human body. The main control performance goal of a HRPI system is that the movement of the robot should adapt to the movements of the human's hand or limb. Therefore, this class of HRPI system is generally a time-varying impedance control system, which includes leader-follower variable impedance control systems, in which the HRPI systems are usually dominated by human interactions. In these systems, such as a rehabilitation robotic system, the role of the human limb and the robot is uncertain, with one periodically supporting the other. As such, in a controlled HRPI system like this, leader-follower roles need to be adjusted accordingly. However, even now, the control of HRPI systems with unspecified leader-follower roles is still challenging; the necessary experimental and theoretical developments are not yet sufficient.

Aimed at physical interaction systems without specified leader-follower roles, this paper studies the design of the CAIC law, as well as its application in the control of the RAPMs. The main contributions of the paper can be summarized as:

(1) For unknown linear systems, a new design method of the AIC law is proposed. The adaptive control method presented in this paper allows the adoption of a regressor with a new structure. This overcomes the limitation of the conventional MRAC method, of which the corresponding non-adaptive *asymptotic* controller is not *necessarily* stable.

(2) A design methodology for coordinated AIC (CAIC) with unspecified leader-follower roles is proposed for controlling the RAPMs. The presented CAIC method can not only overcome the irregular antagonistic forces caused by the kinematic model uncertainties of a RAPM (see Section VI and the Experimental Video 1), but also provides a new solution for the real-time control of a manipulator with super redundant DOFs (see the Experimental Video 2).

(3) The presented CAIC law is validated through a 2-DOF parallel mechanism actuated by three steel wires, with comparison of the performance of the system with the pure kinematic control. The high bandwidth and adjustable output performance of the RAPMs under the CAIC method have also been demonstrated (see Section VI).

The rest of the paper is organized as follows. Section II introduces the dynamic models of the experimental platform. Section III presents the AIC method for a class of uncertain linear systems. The design method of CAIC is presented in Section IV. Some numerical simulation results for illustrating the selection method of control parameters of the closed-loop systems are provided in Section V. In Section VI, we present the experimental results. Conclusions are summarized in Section VII.

II. THE DYNAMICS OF THE EXPERIMENTAL PROTOTYPE

The experimental platform used within this paper is a parallel mechanism element of a snake-like manipulator [60] (see Fig.1), which is a 2-DOF parallel mechanism with a central support.

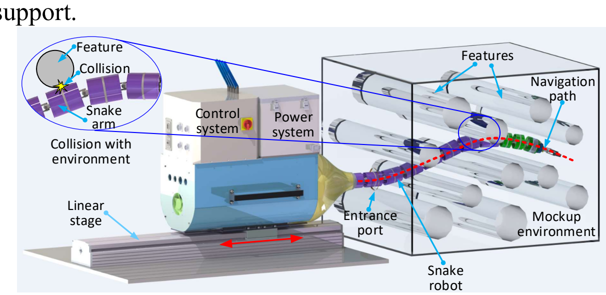

Fig.1 An example working model of a snake-like manipulator for the small-entrance & narrow-space operation. Note: due to the unexpected features of the confined space and low kinematic accuracy of the system, snake-like manipulator is easy to be collided/contacted with the environment, seen the enlarged view

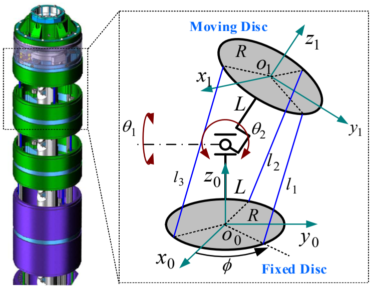

Fig. 2 Schematic diagram of the mechanism element of a snake-like manipulator.

The schematic diagram of the mechanism is shown in Fig. 2. The moving and fixed platforms of the parallel mechanism are connected by a universal joint and driven by three steel wires, which are equally spaced around the circular discs. Where, θ_1 and θ_2 are the joint angles of the center hinge, l_i , $i=1,2,3$ are the effective lengths of the driving steel wires. Two coordinate frames $o_0-x_0y_0z_0$ and $o_1-x_1y_1z_1$ are attached to the center of the two discs respectively, as shown in Fig. 2. The homogeneous transformation matrix from the moving coordinate frame $o_1-x_1y_1z_1$ to the fixed coordinate frame $o_0-x_0y_0z_0$ can be written as

$$T_{o_i}^{o_{i-1}}=\begin{bmatrix} c\theta_1 & -s\theta_1 s\theta_2 & -s\theta_1 c\theta_2 & -Ls\theta_1 c\theta_2 \\ 0 & c\theta_2 & -s\theta_2 & -Ls\theta_2 \\ s\theta_1 & c\theta_1 s\theta_2 & c\theta_1 c\theta_2 & Lc\theta_1 c\theta_2+L \\ 0 & 0 & 0 & 1 \end{bmatrix} \tag{1}$$

where $c(\cdot)$ and $s(\cdot)$ denote the trigonometric functions " cos " and " sin "respectively, L is the length of a half of the cross hinge, which has a symmetric structure, and the radius of the discs is R .

Due to the large number of DOFs (usually greater than 20) and their corresponding actuators of snake-like manipulators, it is difficult to maintain the desired real-time performance when using the traditional control laws [12]-[13]. At the same time, to avoid the irregular increase of the internal forces of the RAPMs (caused by parasitic feedback effects because of the inaccuracy of the kinematic model), this paper investigates the coordinated control method of the RAPMs with unspecified leader-follower roles of the actuators. Therefore, in the following we need to establish the dynamic model of a single segment of the parallel mechanism [61], as shown in Fig.3. The dynamic model of a single segment can be written as

$$M\ddot{l}_i+D\dot{l}_i+Kl_i+G=F_{ei}+F_{ci}+F_i,\quad i=1,2,3 \tag{2}$$

where M , D and K are the uncertain mass, damping and stiffness of the 1-DOF system respectively; G is the uncertain gravity; F_{ei} and F_{ci} are the unknown external load and damping force, respectively, and l_i the effective length of the steel wires, which are also the controlled variable; $u_i=F_i$ is the actuation force. If $e_i=l_i-l_i^d$ is defined as the length error of the steel wire, then the desired closed-loop impedance system can be presented as

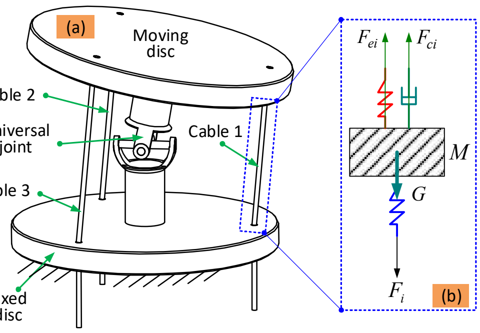

Fig.3 Mechanical model of the 2-DoF manipulator: (a) is the structure of the 2-DoF segment with 3 driving cables; (b) is the mechanical model of a typical driving cable.

$$\overline{M}\ddot{e}_i+\overline{D}\dot{e}_i+\overline{K}e_i=F_{ei},\quad i=1,2,3 \tag{3}$$

where $\overline{M}$, $\overline{D}$ and $\overline{K}$ are the desired inertia, damping and stiffness respectively. As a second order linear system, the impedance parameters $(\overline{M},\overline{K},\overline{D})$ of the desired dynamic system (3) can be determined by the pole assignment theory. When the desired impedance system (3) is stable, it follows that $\ddot{l}_i^d=0$ and $\dot{l}_i^d=0$. Then from (2) and (3) we will have

$$\Delta_M\ddot{e}_i+\Delta_D\dot{e}_i+\Delta_K e_i=-Kl_i^d-G+F_i,\quad i=1,2,3 \tag{4}$$

where $\Delta_M=M-\overline{M}$, $\Delta_D=D-\overline{D}$ and $\Delta_K=K-\overline{K}$. We define $x_1=e_i$ and $x_2=ke_i+\dot{e}_i$, where $k>0$ a constant, and $u_i=F_i$. Then the dynamics (4) is expressed as

$$\begin{aligned} \dot{x}_1 &= -kx_1+x_2 \\ \dot{x}_2 &= -k^2x_1+kx_2 \\ &\quad -\Delta_M^{-1}\left[\Delta_D(-kx_1+x_2)+\Delta_K x_1+Kl_i^d+G\right]+\Delta_M^{-1}u_i \end{aligned} \tag{5}$$

where $i\in\{1,2,3\}$. For the clarity, the uncertain system (5) can be rearranged as following normal form

$$\dot{x}_1=-kx_1+x_2,\qquad \dot{x}_2=\omega_2 u_i+\varphi(x)^{\mathrm{T}}\omega_1 \tag{6}$$

where $\omega_1\in\Re^3$ and $\omega_2\in\Re$ are the unknown parameters, which are given by

$$\omega_1=\begin{bmatrix}\omega_{11}\\ \omega_{12}\\ \omega_{13}\end{bmatrix}=\begin{bmatrix} -\Delta_M^{-1}\left(Kl_i^d+G\right) \\ -k^2+k\Delta_M^{-1}\Delta_D-\Delta_K \\ k+\Delta_M^{-1}\Delta_D \end{bmatrix},\ \text{and}\ \ \omega_2=\Delta_M^{-1} \tag{7}$$

respectively, while the vector $\varphi(x)\in R^3$ is given by $\varphi(x)^{\mathrm{T}}=[1\quad x_1\quad x_2]$.

Remark 1**:** The uncertain system (6) can be regarded as a second-order linear system with unknown disturbances $\varphi(x)^{\mathrm{T}}\omega_1$ and unknown control direction ω_2 . If a control law $u_i(t)$ could be designed to ensure that the unknown disturbance $\varphi(x(t))^{\mathrm{T}}\omega_1(t)$ is *uniformly bounded*, then the closed-loop system of the system (6) is globally asymptotically stable at the equilibrium by correctly selecting the desired impedance parameters $\overline{M}$, $\overline{K}$ and $\overline{D}$. In other words, the position error satisfies $\lim_{t\to\infty} e_i(t)=\overline{K}^{-1}F_{ei}$ while $\lim_{t\to\infty}\ddot{e}_i(t)=\lim_{t\to\infty}\dot{e}_i(t)=0$ when the impedance parameters are properly chosen according to the pole assignment theory.

Remark 2: When the error dynamics (4) is transformed into the state space equation (5), the state variables are defined in a non-traditional manner, namely, $x_1=e_i$ and $x_2=ke_i+\dot{e}_i$. This makes proving proposition 1 in the next section more convenient. In actuality, for the uncertain linear system (4), the adaptive control law presented by Proposition 1 is still feasible under the conventional definition of the state variables $x_1=e_i$ and $x_2=\dot{e}_i$ [58]-[59]. This is because if the systems $\dot{x}_1=x_2,\dot{x}_2=-\overline{K}x_1-\overline{D}x_2$ are taken as the target closed-loop system, it will be globally asymptotically stable by reasonably selecting the feedback parameters $(\overline{K},\overline{D})$, when the control law $u_i(t)$ is designed so that the uncertainty term $\varphi(x)^{\mathrm{T}}\omega_1$ in (6) is uniformly bounded.

III. The AIC law for single actuators

In order to establish the update law of the estimated value of the unknown parameters ω_1 and ω_2 of the uncertain system (6), we construct the following two smooth functions

$$\beta_1(x) = \gamma_1 \int_0^{x_2} \varphi(x_1, \chi) d\chi \tag{8}$$

$$\beta_2(x, \hat{\omega}_1) = \gamma_2 \int_0^{x_2} \left[\bar{K}x_1 + \bar{D}\chi + \varphi(x_1, \chi)^{\mathrm{T}} (\hat{\omega}_1 + \beta_1(x_1, \chi)) \right] d\chi \tag{9}$$

where $\hat{\omega} = \left[\hat{\omega}_1^{\mathrm{T}}, \hat{\omega}_2\right]^{\mathrm{T}}$ is the estimation of the unknown parameters $\omega = \left[\omega_1^{\mathrm{T}}, \omega_2^{-1}\right]^{\mathrm{T}}$, γ_1 and γ_2 are two positive constants. We define the following two error signals with regard to the estimation and the unknown parameters

$$z_1 = \hat{\omega}_1 - \omega_1 + \beta_1(x) \tag{10}$$

$$z_2 = \hat{\omega}_2 - \omega_2^{-1} + \beta_2(x, \hat{\omega}_1) \tag{11}$$

then the following result can be presented.

***Proposition 1*:** For the uncertain system (6), applying the following adaptive control law

$$\dot{\hat{\omega}} = -\left(I + \frac{\partial \beta(x)}{\partial \hat{\omega}}\right)^{-1} \left(\frac{\partial \beta(x)}{\partial x_1}(-kx_1 + x_2) - \frac{\partial \beta(x)}{\partial x_2}\left(\bar{K}x_1 + \bar{D}x_2\right) \right) \tag{12}$$

$$u_i = -\left(\hat{\omega}_2 + \beta_2(x, \hat{\omega}_1)\right)\left(\bar{K}x_1 + \bar{D}x_2 + \varphi(x)^{\mathrm{T}}(\hat{\omega}_1 + \beta_1(x))\right) \tag{13}$$

where $\beta = \left[\beta_1^{\mathrm{T}}, \beta_2\right]^{\mathrm{T}}$ with the constants $\gamma_1 > 0$ and $\gamma_2 > 0$; I is the identity matrix, and $k > 0$ in (12). Then the closed-loop system (6),(12),(13) is globally stable at equilibrium $(x, \hat{\omega}) = (0, \omega)$ and $\lim_{t \to \infty} x(t) = 0$ holds.

Proof. Let $z = \left[z_1^{\mathrm{T}}, z_2\right]^{\mathrm{T}}$ be the estimation errors, which are given by (10),(11), the time derivative of estimation errors z can be written as

$$\begin{aligned} \dot{z} = &\left(I + \frac{\partial \beta(x)}{\partial \hat{\omega}}\right)\dot{\hat{\omega}} + \frac{\partial \beta(x)}{\partial x_1}(-kx_1 + x_2) \\ &+ \frac{\partial \beta(x)}{\partial x_2}\left(\omega_2 u_i - \varphi(x)^{\mathrm{T}} z_1 + \varphi(x)^{\mathrm{T}}(\hat{\omega}_1 + \beta_1(x))\right) \end{aligned} \tag{14}$$

By simultaneously adding and subtracting the term $\frac{\partial \beta(x)}{\partial x_2}\left(\bar{K}x_1 + \bar{D}x_2\right)$ in the right-hand side of (14), it follows that

$$\begin{aligned} \dot{z} = &\left(I + \frac{\partial \beta(x)}{\partial \hat{\omega}}\right)\dot{\hat{\omega}} + \frac{\partial \beta(x)}{\partial x_1}(-kx_1 + x_2) - \frac{\partial \beta(x)}{\partial x_2}\left(\bar{K}x_1 + \bar{D}x_2\right) \\ &+ \frac{\partial \beta(x)}{\partial x_2}\left(\bar{K}x_1 + \bar{D}x_2 + \omega_2 u_i - \varphi(x)^{\mathrm{T}} z_1 + \varphi(x)^{\mathrm{T}}(\hat{\omega}_1 + \beta_1(x))\right) \end{aligned} \tag{15}$$

Let the sum of the first three terms of the right-hand side of (15) equals to zero, namely

$$\left(I + \frac{\partial \beta(x)}{\partial \hat{\omega}}\right)\dot{\hat{\omega}} + \frac{\partial \beta(x)}{\partial x_1}(-kx_1 + x_2) - \frac{\partial \beta(x)}{\partial x_2}\left(\bar{K}x_1 + \bar{D}x_2\right) = 0 \tag{16}$$

then the update law (12) can be obtained from (16), while (15) follows that

$$\begin{aligned} \dot{z} = &\frac{\partial \beta(x)}{\partial x_2}\left(\bar{K}x_1 + \bar{D}x_2\right) \\ &+ \frac{\partial \beta(x)}{\partial x_2}\left(\omega_2 u_i - \varphi(x)^{\mathrm{T}} z_1 + \varphi(x)^{\mathrm{T}}(\hat{\omega}_1 + \beta_1(x))\right) \end{aligned} \tag{17}$$

By applying (8) and (9), note that

$$\frac{\partial \beta_1(x)}{\partial x_2} = \gamma_1 \varphi(x) \tag{18}$$

$$\frac{\partial \beta_2(x, \hat{\omega}_1)}{\partial x_2} = \gamma_2 \left[\bar{K}x_1 + \bar{D}x_2 + \varphi(x)^{\mathrm{T}}(\hat{\omega}_1 + \beta_1(x))\right] \tag{19}$$

and define

$$\Phi(x, \hat{\omega}_1) := \begin{bmatrix} \gamma_1^{-1} \partial \beta_1(x)/\partial x_2 \\ \omega_2 \gamma_2^{-1} \partial \beta_2(x, \hat{\omega}_1)/\partial x_2 \end{bmatrix} \tag{20}$$

then by substituting (18)-(20) into (17), one obtains

$$\dot{z} = \Lambda \Phi(x, \hat{\omega}_1) \left[-\varphi(x)^{\mathrm{T}} z_1 + \omega_2 u_i + \gamma_2^{-1} \frac{\partial \beta_2(x, \hat{\omega}_1)}{\partial x_2} \right] \tag{21}$$

where $\Lambda = \begin{bmatrix} \gamma_1 & 0 \\ 0 & \gamma_2 \omega_2^{-1} \end{bmatrix}$. By using (11) and the control law (13), then (21) can be simplified as

$$\dot{z} = -\Lambda \Phi(x, \hat{\omega}_1) \Phi(x, \hat{\omega}_1)^{\mathrm{T}} z \tag{22}$$

Consider the function $U(z) = z^T \Lambda^{-1} z$, whose time derivative along the system (22) satisfies

$$\dot{U}(z) = -2\left(\Phi(x, \hat{\omega}_1)^{\mathrm{T}} z\right)^2 \le 0 \tag{23}$$

which means $z(t) \in L_\infty$ and $\Phi(x(t), \hat{\omega}_1(t))^{\mathrm{T}} z(t) \in L_2$. Note that the closed-loop system (6),(12),(13) can be represented as

$$\dot{x}_1 = -kx_1 + x_2, \qquad \dot{x}_2 = -\left(\bar{K}x_1 + \bar{D}x_2\right) - \Phi(x, \hat{\omega}_1)^{\mathrm{T}} z \tag{24}$$

This is an asymptotically stable linear system perturbed by a bounded signal $\Phi(x, \hat{\omega}_1)^{\mathrm{T}} z \in L_2$. For the extended system (22) and (24), if we select the following Lyapunov function

$$V(x, z) = \bar{K}x_1^2 + x_2^2 + \bar{D}^{-1} U(z)$$

then the time-derivative of it along the extended system (22) and (24) can be given as

$$\begin{aligned} \dot{V}(x, z) &= -k\bar{K}x_1^2 - 2\bar{D}x_2^2 - 2x_2 \Phi(x, \hat{\omega}_1)^{\mathrm{T}} z - 2\bar{D}^{-1}\left(\Phi(x, \hat{\omega}_1)^{\mathrm{T}} z\right)^2 \\ &= -k\bar{K}x_1^2 - \bar{D}^2 x_2^2 - \bar{D}^{-1}\left(\Phi(x, \hat{\omega}_1)^{\mathrm{T}} z\right)^2 \\ &\quad - \left(\sqrt{\bar{D}}\, x_2 + \sqrt{\bar{D}^{-1}}\, \Phi(x, \hat{\omega}_1)^{\mathrm{T}} z\right)^2 \le 0 \end{aligned} \tag{25}$$

Thus, the extended system (22) and (24) has a globally stable equilibrium at the origin $(x, z) = (0, 0)$, while the closed-loop system (6),(12), (13) has a globally stable equilibrium at $(x, \hat{\omega}) = (0, \omega)$. By LaSalle's invariance principle, all trajectories of the closed-loop system converge to the invariant set

$$\Omega = \left\{(x, z) \in \Re^2 \times \Re^4 : x = 0, \Phi(x, \hat{\omega}_1)^{\mathrm{T}} z = 0\right\} \tag{26}$$

Therefore, the condition $\lim_{t \to \infty} x(t) = 0$ holds. This completes the proof.

***Remark 3*:** It should be mentioned that, by constructing the smooth functions $\beta_1(x)$ and $\beta_2(x, \hat{\omega}_1)$, a dynamic system for the estimation errors z can be established (14). This also enables us to establish the update law (12) for the adaptive control system based on (16). This novel approach should be compared to the classical MRAC approach, in which the estimation errors (10) and (11) with $\beta_i = 0$ are only guaranteed to be bounded and converging to certain unknown constants, while the transient behavior of the closed-loop system may be unacceptable. However, for the closed-loop system (24) with the adaptive control law (12), (13), the disturbance term $\Phi(x(t), \hat{\omega}_1(t))^{\mathrm{T}} z$ in the closed-loop system (24) is *uniformly bounded*, satisfying the condition $\Phi(x, \hat{\omega}_1)^{\mathrm{T}} z \in L_2$. Therefore, when the time tends to infinity, the disturbance term $\Phi(x, \hat{\omega}_1)^{\mathrm{T}} z \in L_2$ tends to zero, and the behavior of the motion of the closed-loop system of the uncertain system (6) gradually tends to that of the following asymptotically stable linear system:

$$\dot{x}_1 = -kx_1 + x_2, \qquad \dot{x}_2 = -\bar{K}x_1 - \bar{D}x_2 \tag{27}$$

under the assumption that the control parameters $(k,\overline{K},\overline{D})$ in (27) are properly chosen according to the pole assignment theory.

Remark 4**:** It is worth mentioning that the coefficient matrix $I+\partial\beta(x)/\partial\hat{\omega}$ in the update law (12) is always reversible since the partial derivative term $\partial\beta(x)/\partial\hat{\omega}$ only contributes to the off-diagonal elements. In addition, it can be seen from the target closed-loop system (27) that linear feedback $-\overline{K}x_1-\overline{D}x_2$ is just used in constructing the function (9). In practical applications, other feedback forms can also be used to construct the target closed-loop system to obtain better performance. This shows that the functions (9) can be constructed flexibly. It can also be seen from equation (22) that when the constant coefficients γ_1 and γ_2 in functions (8) and (9) take larger values, it accelerates the convergence of the estimation error $z(t)$. This enables the reduction of the settling-time of the target closed-loop system (24), which is advantageous for the practical application of the developed adaptive control law (12) and (13). This point should also be compared to the classical MRAC approach, where the control gains of the update law does not necessarily speed-up the response of the closed-loop system, since the update law in MRAC approach is generally designed to cancel out the terms about the estimation errors in the time derivative function of a Lyapunov function. However, in Proposition 1, the update law is designed to make the perturbation term uniformly bounded, i.e., $\Phi(x,\hat{\omega}_1)^{\mathrm{T}}z\in L_2$.

IV. CAIC FOR THE MULTI ACTUATORS OF THE RAPMS

A. *The coordination constraints*

The AIC method directly provides a feasible way for compliant and coordinated motion control within the actuation space of a parallel mechanism. The general constraints that should be satisfied by the coordinated motion of the multiple actuation systems include the internal force constraints and associated motion constraints. For a RAPM with m independent actuators, the force constraints of the actuators can generally be expressed as

$$f(F_{e1},\cdots,F_{em})\le\Gamma_0(t) \tag{28}$$

where $\Gamma_0(t)\in R^6$ is the given wrench, and F_{ei} is the external load of the *i*-th actuator. The associated motion constraints can generally be expressed as

$$p(l_1,\cdots,l_m)=\Theta(t) \tag{29}$$

which includes both the kinematic constraints, and the task constrains of the RAPMs, where $\Theta(t)$ denotes the given trajectories, which can be specified either in the configuration space or the operation space of the RAPMs, $l_1,\cdots,l_m$ express the controlled variables of a RAPM in its actuation space. For the RAPM shown in Fig.3, the compound constraints of the force-motion can be specified as

$$\begin{cases}\sum_{i=1}^{3}F_{ei}\le F_0(t)\\ F_{ei}+F_{preload}>0,\text{for } i=1,2,3\\ \sum_{i=1}^{3}\left(\mathrm{R}F_{ei}\right)\le\tau_0(t)\end{cases} \tag{30}$$

$$p(l_1,l_2,l_3)=\Theta(\theta_1(t),\theta_2(t)) \tag{31}$$

where $F_0(t)$ is the resultant force of the three steel wires; R is the force-arm of the steel wires applying on the moving disc; $\tau_0(t)$ is the output torque of the RAPM; $\Theta(\theta_1(t),\theta_2(t))$ is the given joint space trajectory of the RAPM specified by given operation tasks; $p(l_1,l_2,l_3)$ is the corresponding trajectory in the actuation space of the RAPM.

B. *Coordinated impedance control of the RAPMs*

For the given operation task constraints (30), (31), the target impedance system is given by (3), and the external load F_{ei} of each actuator is bounded, then a set of appropriate impedance parameters $(\overline{M},\overline{D},\overline{K})$ can be selected to make the dynamic system (3) globally asymptotically stable at the equilibrium. Referring to the uncertain dynamic system (4), in which the target impedance system is considered, the expected output force of each actuator no longer explicitly appears in the controlled system (4). Therefore, under the action of the adaptive controllers (12), (13), even though the dynamics of each actuation system is almost unknown, it can be asymptotically stably controlled to its corresponding target closed-loop system (27) as long as the given motion trajectory is feasible. By reasonably selecting the control parameters $(k,\overline{D},\overline{K})$, the target closed-loop system (27) is also globally asymptotically stable for all actuators of the RAPMs. Based on the above analysis, we can deduce the following proposition:

Proposition 2**:** For the uncertain dynamic system (4), if the given task constraints (30), (31) are feasible and each actuator adopts the adaptive impedance control laws (12) and (13), the coordinated control system (4), (12), and (13) is globally practically stable.

Remark 5**:** The global practical stability here means that since the coordinated control is implemented in the actuation space of the RAPM, even if the position error e_i of each actuator is globally asymptotically stable, the error between the actual motion and planned motion will still exist in the inaccurate system kinematics model (31). The motion planning errors cannot be eliminated by the coordinated motion control in the actuation space of the RAPMs. However, in practical applications, the motion planning errors are usually bounded, and requiring the new approaches to be developed to reduce the motion planning errors.

Remark 6**:** By implementing CAIC in the actuation space, the internal antagonistic forces between the actuators of the RAPMs can be effectively controlled. By properly selecting the desired impedance parameters $(\overline{M},\overline{D},\overline{K})$ of the desired impedance system (3), the dynamic characteristics of each actuator of the RAPMs at their equilibrium are similar to a group of parallel passive mass-spring-damping systems. The main reasons to obtain stable and compliant motion control are: 1) the impedance control is implemented for each actuator; and 2) the adaptive controller is adopted to overcome the uncertainties of the system model. In particular, the adaptive control laws (12) and (13) have been developed for the unknown systems (4), thus the difficulty in establishing an accurate dynamic model of the RAPMs can be effectively reduced, while avoiding an irregular increase of the internal antagonistic forces caused by any inaccuracies in the RAPM's kinematic model.

V. Numerical Simulations

In this section, the AIC system on a single actuator is numerically simulated as a case study to investigate the closed-loop performance of the controlled systems. Here it is assumed that the mass of the mechanical model given by Fig.3 is $M=5\text{Kg}$, the damping in the model is D=100Nm/s, and the equivalent stiffness is $K=4\times10^{3}\,\text{N/m}$. We also assume the initial state errors of the controlled system (6),(12), and (13) are given by $(e_i,\dot{e}_i)=(0.025\text{m},0\text{m/s})$; the unknown gravity in the model is $G=-10\text{N}$; the unknown external load is $F_{ei}(t)=5\sin(20\pi t)+\cos(10\pi t-\pi/9)$ N. When the feedback control parameters are selected as $(k,\overline{M},\overline{D},\overline{K})=(0,0.5\text{Kg},20Ns/m,200N/m)$, the coefficients of the functions (8) and (9) are chosen as $(\gamma_1,\gamma_2)=(20,20)$, and the initial values of the estimation parameters are given by $\hat{\omega}(0)=[0,0,0,0]^{\mathrm{T}}$, a numerical simulation result for the position stabilization of the single actuator are illustrated in Fig.4.

Referring to the simulation results, it can be observed that in the simulation period of 4 seconds, it is assumed that the unknown gravity G always exists and the unknown external load $F_{ei}(t)$ appears between the second and third seconds (see Fig.4(d)). It can be seen from Fig.4(a), when the unknown load remains unchanged, the state responses of the system are asymptotically stable; while when the external load changes, the state responses are stable. Comparing Fig.4(a) and Fig.4(c), it can be seen that when the estimation parameters are not stable at the start stage (the first 0.5s), the state responses of the closed-loop system have a certain fluctuation, and the corresponding driving force (Fig.4(b)) also has a certain oscillation. When the estimated parameters are stable, the response of the adaptive closed-loop control systems (6), (12), and (13) is similar to a passive spring. When a dynamically external force is exerted, the system states will produce certain position and speed errors to adapt to the changes of the external force, so that the driving force of the closed-loop system is always bounded.

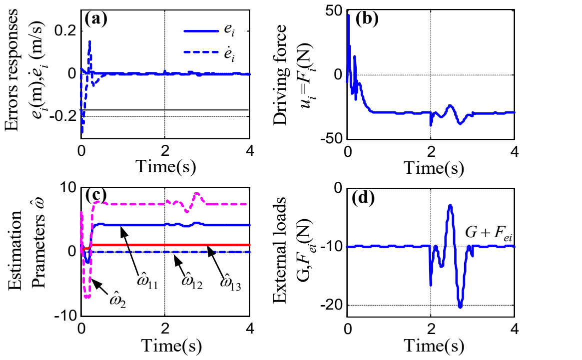

Fig.4 Simulation results of the AIC based control system for single actuator. (a)State responses of the controlled system (6); (b) Driving force of the controlled system; (c) The responses of estimation parameters; (d) Uncertain gravity and the external load of the controlled system (6)

The passive spring-like character of the closed-loop impedance control system makes it particularly suitable for the coordinated control of multi-mechanical systems under compound constraints associated with the force and position. The adaptive control method gives the closed-loop system exceptionally robust stability against the uncertainties of the system model. Therefore, it is suitable for achieving motion control of a RAPM in the actuation space. Even if inaccurate motion commands are received from an inaccurate system kinematics model, the AIC system can help the RAPM avoid abnormal antagonistic internal forces and excessive/sudden changes of the environmental contact force.

VI. Experiments

A. Experimental prototype and the structure of the AIC law

In this paper, the CAIC law with the following structure is used to control the RAPM prototype, which is illustrated in Fig.5. Where, $\theta_1^d(t)$ and $\theta_2^d(t)$ are the given trajectories in joint space, and $l_i^d(t)$, $i=1,2,3$ are the target movement trajectories in the actuation space. The AIC law (13) gives the tension control command $u_i(t)$, which corresponds to the configuration motion space of RAPM mechanism. f_i^d is the given preload of the i-th steel wire. The vector space of the preload forces is orthogonal to the motion space of the parallel mechanism and has no influence on the movements of the parallel mechanism, but the preload force can be used to eliminate the clearances of the transmission systems to improve the trajectory tracking accuracy of the RAPMs, or to improve the output stiffness and the load carrying capacity of the RAPMs. The sum of the output $u_i(t)$ of the AIC law and the preload forces are used as the nominal actuation forces, and the errors between them and the actual tensions of the steel wires are used as the error inputs of the force-PID controller. The outputs of the force-PID controllers are used to generate the PWM control commands for the DC servo motors of the RAPM. The overall closed-loop controller for the experimental prototype is in the actuation space but with the double feedback of the force and position.

Fig.6 shows the 2-DOF RAPM experimental platform. The parallel mechanism is driven by three DC servo motors (type: Maxon-RE30). The transmission elements are constructed by screw-nut pairs. The moving disc of the RAPM is driven by three equally spaced steel wires. Each steel wire is equipped with a tension sensor (type: AT8202, measuring range: 0-5kN). The controller hardware of the experimental platform is based on a NI myRIO-1900 control board (National Instruments Corp.). The frequency of the FPGA-based control board is 40MHz. The control board has several encoder interfaces, analog signal acquisition and digital I/O interfaces. The control law of the experimental system is developed by applying mix-programming of LabVIEW and MATLAB software. The control command cycle used in the experiments is 10 milliseconds [62].

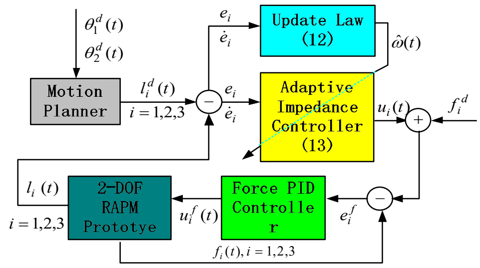

Fig.5 The structure of the CAIC law

The CAIC law illustrated in Fig.6 adopts a double-loop structure, in which the position control is the outer loop, while the force control is the inner loop. By adjusting the control parameters of the double feedback loops, the controller can not only realize position-based CAIC, but also realize the tension-based CAIC. In Section 6C and Section 6D, the corresponding experimental results are presented for the two kinds of control tasks respectively.

To minimize the impact of the external disturbances (e.g. creeping of the driving cable, static friction direction between driving cable and guiding hole) on the 2-DOF manipulator, the calibration procedure is repeated for each test, which can be summarized as the following steps: 1) a cylinder (same diameter with the manipulator and sliced into two symmetrical grooves) is used to straighten the 2-DOF manipulator; 2) three motors are driven synchronously to increase the tension of the driving cables, aided with the real-time closed-loop controllers to achieve the desired tensions (i.e., force sensors are attached at the driving cables to feedback the real-time tension); 3) cylindrical supports are removed after the desired tensions of the driving cables is attained; 4) perform the planned motions of upper platform with the help of the developed CAIC.

For the calibration of the multiple-DoFs manipulator (also called a snake-line robot, see Experimental Video 2), a similar procedure with the 2-DOF manipulator is adopted. The difference is that a longer split support cylinder will be used to straighten the manipulator prior to calibration. Then the calibration procedure of the 2-DOF manipulator is repeated (i.e., from base to tip) on all the sections to regulate the tension of the driving cables to the desired values.

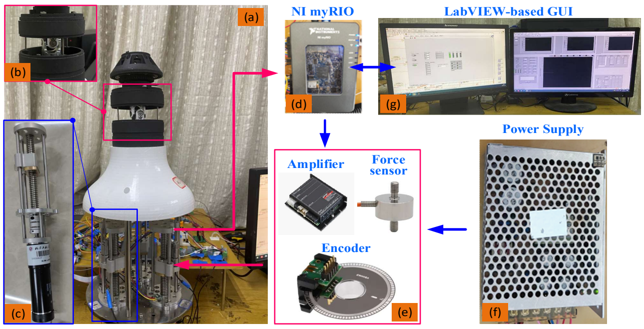

Fig.6 The experimental setup of the 2-DoF manipulator: (a) is the 2-DoF manipulator; (b) is the structure of the universal joint actuated the driving cables; (c) is the structure of the linear motor unit; (d) is the microprocessor for implementing the developed algorithm; (e) is the actuation and sensor components used in the system; (f) is the power supply; (g) is the LabVIEW-based GUI design for the easy operation

B. Pure position trajectory control of the 2-DOF RAPM

Assuming the joint space trajectory of the 2-DOF RAPM is given by

$$\begin{cases} \theta_1(t) = \pi \sin(2\pi t/50)/9 \\ \theta_2(t) = \pi \sin(4\pi t/50)/9 \end{cases} \tag{32}$$

the corresponding effective length of the steel wires can be calculated by

$$l_i(t) = \sqrt{\left\| P_{A_i}^{o_0} - P_{B_i}^{o_0} \right\|}, \; i = 1,2,3 \tag{33}$$

where $P_{A_i}^{o_0}$ denotes the homogeneous coordinate of the fixed point A_i of the i-th steel wire attached on the movable disc, $P_{B_i}^{o_0}$ is the homogeneous coordinate of the passing point of the i-th steel wire attached on the fixed disc. The two points are all represented in the frame $o_0 - x_0 y_0 z_0$. The homogeneous coordinate of the point $P_{A_i}^{o_0}$ is calculated by

$$P_{A_i}^{o_0} = T_{o_1}^{o_0} P_{A_i}^{o_1} \tag{34}$$

where $T_{o_1}^{o_0}$ is given by (1), while $P_{A_i}^{o_1}$ is given by

$$P_{A_i}^{o_1} = P_{B_i}^{o_0} = \begin{bmatrix} \mathrm{R}\cos(\phi + 2\pi(i-1)/3) \\ \mathrm{R}\sin(\phi + 2\pi(i-1)/3) \\ 0 \\ 1 \end{bmatrix} \tag{35}$$

where R is the disc's radius of the 2-DOF RAPM, ϕ is the offset angle of the first steel wire with regard to the axis x_0, while the spacing angle between adjacent steel wires are $2\pi/3$.

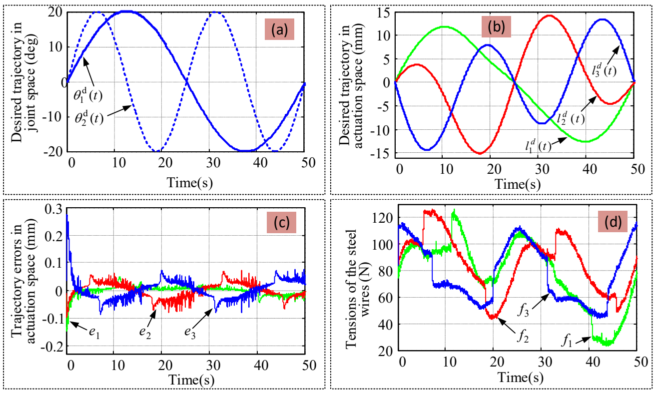

Fig.7 (a) to (d) are the joint space trajectories of the 2-DOF RAPM given by (32), actuation space trajectories of the 2-DOF RAPM given by (33), position trajectory errors of the 2-DOF RAPM in actuation space, and tension in the steel wires in the 2-DOF RAPM in the position trajectory tracking task, respectively.

The joint space trajectories of the 2-DOF RAPM given by (32) are illustrated in Fig.7 (a). The corresponding actuation space trajectories are shown in Fig.7 (b). For the PID controller with just the position error feedback, Fig.7 (c) illustrates an example trajectory tracking result by adjusting the feedback parameters and the preload force (in this experiment, the preload of the three steel wires is about 100N, respectively). It can be seen from Fig.7 (c), besides the larger initial position errors, the trajectory tracking accuracy of the experimental prototype in the actuation space can be controlled within $\pm 0.1\mathrm{mm}$. Theoretically, this position accuracy of the steel wires relates to the joint angle error of about $\pm 0.15^{\circ}$ (as the length of the force-arm of the driving steel wires in the experimental prototype is $\mathrm{R} = 33.5\mathrm{mm}$). Fig.7 (d) shows the measurement results of the force sensors during the position trajectory tracking (in this experiment, tensions are also measured for comparison). It can be seen from Fig.7 (d) that the tension of the three wires is greater than zero throughout the time period of the given trajectory tracking task. This indicates that there is no slack in the driving wires. However, as shown by Fig.7 (d), the tension of the three steel wires experiences several jumps. With the repeat experiments and in-depth analysis, we believe that the tension jump is caused by the Coulomb friction in the transmission system of the experimental prototype. By comparing Fig.7 (b) to Fig.7 (d), it can be seen that the tension jumps normally occur at the local vertex of the wires' position trajectories. At these points, the direction of the steel wires' movement will switch to the opposite direction, causing hysteresis effects in the tension of the steel wires due to the Coulomb friction of the transmission system.

C. Position based CAIC of the 2-DOF RAPM

Whilst using the CAIC control law shown in Fig.6, the control parameters of the adaptive impedance controller are set with larger values in this experiment than previously. Specifically, it is set with $(\overline{K},\overline{D})=(170{,}170)$; the feedback parameters of the update law are selected as $(\gamma_1,\gamma_2)=(20{,}20)$; the initial values of the uncertain parameters $\hat{\omega}^i(0)\in\Re^4, i=1,2,3$ are given as $(0{,}0{,}0{,}300)^{\mathrm{T}}$, where the superscript "i" represents the i-th actuator. We also set the PID control parameters of the force feedback loop to smaller values $(k_I^f,k_P^f,k_d^f)=(0{,}10{,}0)$. In this experiment, the preload of the three steel wires is also set to about 100N.

Applying the CAIC in the actuation space of the parallel mechanism, each motor of the parallel mechanism actuates the steel wire to track the trajectory shown in Fig.11. In other words, the motion constraints are given by (32) and (33), while the force constraints are given by

$$\begin{cases}\sum_{i=1}^{3} F_{ei}\le 500\mathrm{N}\\ F_{ei}+F_{preload}>10\mathrm{N},\ \text{for } i=1,2,3\\ \sum_{i=1}^{3}(\mathrm{R}F_{ei})=0\mathrm{Nm}\end{cases} \tag{36}$$

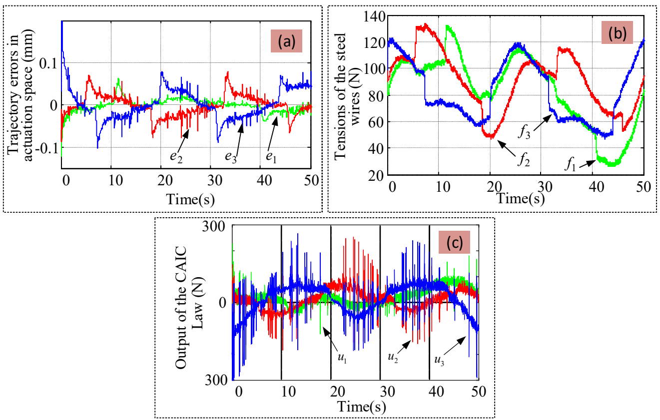

Fig.8 (a) to (c) are the position trajectory errors, tension of the steel wire, and outputs of the position-based CAIC law of the 2-DOF RAPM under position-based CAIC, respectively.

The obtained position trajectory tracking errors are shown in Fig.8 (a). It can be seen that the effects of position tracking errors are close to the result presented by Fig.8 (b). By further comparing the tension trajectories shown in Fig.8 (b) and Fig.7 (d), it can be found that the tension trajectories of the steel wires under the two control modes are similar. This reveals that the mechanical characteristics of the transmission system of the parallel mechanism are not regulated when the position trajectory accuracy is the main control target. It can also be observed from Fig.8 (c) that, in the process of position trajectory tracking, the outputs of the position-based AIC laws are continuously adjusted at high frequency in order to achieve the high position trajectory tracking accuracy, so that the parallel mechanism shows high output stiffness.

D. Tension based CAIC of the 2-DOF RAPM

In this experiment, the CAIC control law shown in Fig.6 is also adopted. The motion constraints (32), (33) and the force constraints (36) stay unchanged. In order to improve the motion performance of the parallel mechanism, the control parameters of the adaptive impedance controller are taken as a set of smaller values $(\overline{K},\overline{D})=(0.1{,}1)$. The feedback parameters of the update law are still set as $(\gamma_1,\gamma_2)=(20{,}20)$, and the initial values of the uncertain parameters $\hat{\omega}^i(0)\in\Re^4, i=1,2,3$ are also set as $(0{,}0{,}0{,}300)^{\mathrm{T}}$. The parameters of the force PID controller are set as a group of larger values $(k_I^f,k_P^f,k_d^f)=(0.004{,}400{,}15)$. The obtained position trajectory tracking errors are shown in Fig.14, while Fig.9 (b) illustrates the tension trajectories of the steel wires and Fig.9 (c) plots the output trajectories of the position-based CAIC law.

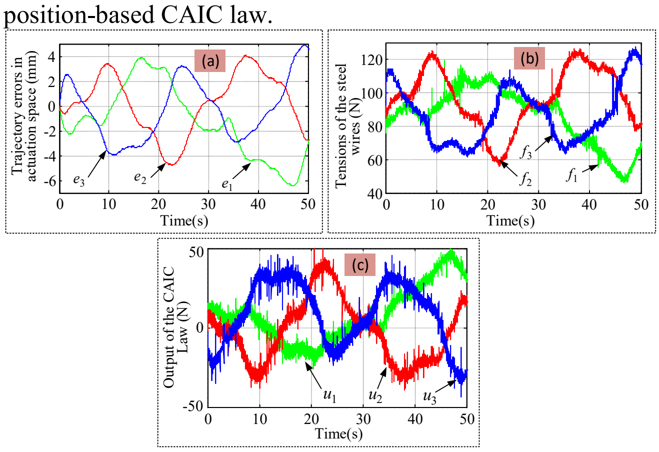

Fig.9 (a) to (c) are the position trajectory errors, tension of the steel wire, and outputs of the position-based CAIC law of the 2-DOF RAPM under position-based CAIC, respectively.

By analyzing the experimental results, it is not difficult to find that, by adjusting the relevant feedback parameters of the CAIC control law, the fluctuation ranges of the AIC law's outputs can be greatly reduced (see Fig.9 (c)), the variation in the tension of the steel wires is reduced (Fig.9 (b)), and the tracking accuracy of the position trajectory is actively adjusted to adapt to the external loads (Fig.9 (a)). Thus, the output stiffness of the RAPM can be actively adjusted by the developed CAIC control law, enabling the system to have improved motion performance. By comparing Fig.9 (b) and Fig.8 (b) it can be found that the Coulomb friction effects shown in the position-based control task have disappeared in the tension-based control task. This reveals that the RAPMs can exhibit good force interaction responsivity with the environment, whether that include human beings or otherwise, whilst maintaining a given motion trajectory. In addition, it is worth pointing out that, with these dynamic characteristics, the RAPM can also have the capability to compensate for the HRPI or robot-environment physical interaction. In terms of potential applications, this complements the control mode presented in section 6C.

VII. Conclusion

In order to improve the performance of conventional snake-like robots (characterized by super redundant DOFs) to adapt to external interactions, a new kind of CAIC has been developed and adapted to RAPMs in this paper. With the newly developed control algorithm and the corresponding experimental results, the innovations can be summarized as follows:

1) A new method for designing the AIC law is proposed for uncertain second order linear systems, and the global asymptotical stability of the closed-loop system has been analyzed. By constructing two integral functions associated with the system state and estimated parameters, the update law of the estimated parameters is established. Instead of using the error cancellation method, the error management method is used to construct the adaptive control law, so that a major limitation of the conventional MRAC method is overcome.
2) A CAIC scheme with unspecified leader-follower roles is proposed for the control of the RAPMs. The presented CAIC law is verified by a set of experiments on a prototype 2-DOF manipulator that is actuated by three equally spaced steel wires. The performance of the system under pure kinematic control and the CAIC methods are compared and analyzed. The high bandwidth and adjustable output performances of the RAPMs under the CAIC method have been demonstrated.
3) Compared with pure kinematics control, the proposed CAIC method can not only realize the motion coordination control with accurate position as the main target with high-precision tracking performance (in our experiments, motion tracking errors of ±0.1 mm is achieved), but also achieve motion coordination control with force output as the main target, so that both the internal and external interactive forces can be controlled within a smaller fluctuation range. Meanwhile, uncertain Coulomb friction effects can be removed from the force transmission characteristics of the RAMPs with our developed algorithm.

The CAIC method proposed in this paper aims to realize the real-time control of snake-like robots (see Experimental Video 2), where the motion coordination control is normally executed in the actuation space of the RAPMs, resulting in difficulty in correcting/compensating for the errors generated by motion planning. To solve this problem, a practical global stability method is developed for CAIC systems.

Methodologies for designing globally asymptotically stable CAIC system are worth studying as a next step. Extending the method for designing the AIC law, as proposed in this paper, to nonlinear systems is also a challenge/worthy investigation for the future study. In addition, constructing finite-time stable [33],[54] CAIC laws for human-machine interaction systems is also an interesting research topic.

References

[1]. L. Wang, J. Wu, J.Wang, et al., "An Experimental Study of a Redundantly Actuated Parallel Manipulator for a 5-DOF Hybrid Machine Tool", *IEEE/ASME Trans. Mechatron.*, vol. 14, no. 1, pp.72-81, Feb. 2009.

[2]. J. Kim, F. C. Park, S. J. Ryu, et al., "Design and Analysis of a Redundantly Actuated Parallel Mechanism for Rapid Machining", *IEEE Trans. Robotics and Automation*, VOL. 17, NO. 4, pp.423-434, Aug. 2001.

[3]. S. Zhong, J. Chen, X. Niu, et al., "Reducing Redundancy of Musculoskeletal Robot With Convex Hull Vertexes Selection", *IEEE Trans. Cognitive and Development Systems*, vol. 12, no. 3, pp.601-617, Sep. 2020.

[4]. Y. Zhao, K. Qian, S. Bo, Z. Zhang, et al, "Adaptive Cooperative Control Strategy for a Wrist Exoskeleton Using Model-Based Joint Impedance Estimation", IEEE*/ASME Trans. Mechatronics*, vol.28, no.2, pp: 748-757, April. 2023.

[5]. M. Deng, Z. Li, Y. Kang, et al., "A Learning-Based Hierarchical Control Scheme for an Exoskeleton Robot in Human–Robot Cooperative Manipulation", *IEEE Trans. Cybernetics*, vol.50, no. 1, pp.112-125, Jan. 2020.

[6]. Y. Huo, X. Li,X. Zhang , X. Li , and D. Sun , "Adaptive Intention-Driven Variable Impedance Control for Wearable Robots With Compliant Actuators", *IEEE Trans. Cont. Sys. Tech.*, vol. 31, no. 3, pp.1308-1323, May 2023.

[7]. X. Wu, Z. Li, Z. Kan, and H. Gao, "Reference Trajectory Reshaping Optimization and Control of Robotic Exoskeletons for Human–Robot Co-Manipulation", *IEEE Trans. Cybernetics,* vol. 50, no. 8, pp.3740-3751, Aug. 2020.

[8]. J. C. P´erez-Ibarra, A. A. G. Siqueira, M. A. Silva-Couto, T. L. de Russo, and H. I. Krebs, "Adaptive Impedance Control Applied to Robot-Aided Neuro-Rehabilitation of the Ankle", *IEEE Robotics and Automation Letter*, vol. 4, np. 2, pp. 185-192, Apr. 2019.

[9]. S. Hussain, S. Q. Xie, and P. K. Jamwal, "Adaptive Impedance Control of a Robotic Orthosis for Gait Rehabilitation", *IEEE Trans.Cybernetics*, vol. 43, no. 3, pp. 1025-1034, Jun. 2013.

[10]. Z. Li, Q. Li, P. Huang, H. Xia, and G. Li, "Human-in-the-Loop Adaptive Control of a Soft Exo-Suit With Actuator Dynamics and Ankle Impedance Adaptation", *IEEE Trans. Cybernetics*, DOI:10.1109/TCYB.2023.3240231.

[11]. J. Yang, T. Sun, L. Cheng, and Z.-G. Hou, "Spatial Repetitive Impedance Learning Control for Robot-Assisted Rehabilitation", *IEEE/ASME Trans. Mechatron.*, vol. 28, no. 3, pp.1280-1290, Jun. 2023.

[12]. A. Müller, "Consequences of Geometric Imperfections for the Control of Redundantly Actuated Parallel Manipulators", *IEEE Trans. Robotics*, vol. 26, no. 1, pp,21-31, Feb. 2010.

[13]. H. Cheng, Y.-K. Yiu, and Z. Li, "Dynamics and control of redundantly actuated parallel manipulators," *IEEE/ASME Trans. Mechatron.*, vol. 8, no. 4, pp. 483-491, Dec. 2003.

[14]. D. Chakarov, "Study of the antagonistic stiffness of parallel manipulators with actuation redundancy", *Mechanism and Machine Theory*, vol.39, pp.583-601, 2004.

[15]. N. Mostashiri, J. S. Dhupia, A. W. Verl, and W. Xu, "A Review of Research Aspects of Redundantly Actuated Parallel Robots for Enabling Further Applications", *IEEE/ASME Trans. Mechatron.*, vol.23, no.3, pp.1259-1269, Jun. 2018.

[16]. J. A. Blaya and H. Herr, Adaptive Control of a Variable-Impedance Ankle-Foot Orthosis to Assist Drop-Foot Gait, *IEEE Trans. Neural Systems and Rehabilitation Engineering*, vol.12, no.1: pp.24-31, 2004.

[17]. J.C. P´erez-Ibarra, A. A. G. S., Marcela A. Silva-Couto, T. L. de Russo, and H. I. Krebs,"Adaptive Impedance Control Applied to Robot-Aided Neuro-Rehabilitation of the Ankle", *IEEE Robotics and Automation Letter*, vol.4, no.2, pp.185-192, Apr. 2019.

[18]. P. K. Jamwal, S. Hussain, et al., "Adaptive Impedance Control of Parallel Ankle Rehabilitation Robot", *ASME Journal of Dynamic Systems, Measurement, and Control*, vol. 139, no.111006, pp.1-7, Nov. 2017.

[19]. Z. Li, ,Z. Huang, W. He, et al., "Adaptive Impedance Control for an Upper Limb Robotic Exoskeleton Using Biological Signals", *IEEE Trans. Industrial Electronics*, vol. 64, no. 2, pp.1664-1674, Feb. 2017.

[20]. B. Huang, Z.Li, X. Wu, et al., "Coordination Control of a Dual-Arm Exoskeleton Robot Using Human Impedance Transfer Skills", *IEEE Trans. Sys. Man and Syb.: Systems*, vol. 49, no. 5, pp.954-963, May. 2019.

[21]. M. Sharifi, S.Behzadipour, and H. Salarieh, "Nonlinear Bilateral Adaptive Impedance Control With Applications in Telesurgery and Telerehabilitation", *ASME Journal of Dynamic Systems, Measurement, and Control*, vol. 138 , no.111010, pp.1-16, Nov.2016.

[22]. T. Su, L. Niu, G. He, et al., "Coordinated variable impedance control for multi-segment cable-driven continuum manipulators", *Mechanism and Machine Theory*, vol.153, no.103969, 2020.

[23]. S. Jung, T. C. Hsia, and R. G. Bonitz, "Force Tracking Impedance Control of Robot Manipulators under Unknown Environment", *IEEE Trans. Cont. Sys. Tech.*, 2004, 12(3): 474-483.

[24]. C. Ott, Cartesian Impedance Control of Redundant and Flexible Joint Robots (Springer Tracts in Advanced Robotics), vol. 49. New York, NY, USA: Springer, 2008.

[25]. P. K. Jamwal, S. Hussain, M. H. Ghayesh, et al., "Impedance control of an intrinsically compliant parallel ankle rehabilitation robot", *IEEE Trans. Industrial Electronics*, 2016, 63(6): 3638-3646.

[26]. C. Ott, R. Mukherjee, Y.Nakamura, "A Hybrid System Framework for Unified Impedance and Admittance Control", *Journal of Intelligent and Robotic Systems*, 2015, 78(3-4): 359-375.

[27]. S. Wolf, G. Grioli, O. Eiberger et al, “Variable Stiffness Actuators: Review on Design and Components”, *IEEE/ASME Trans. Mechatron.*, vol.21, no.5, pp: 2418-2430, Oct. 2016.
[28]. L. Liu, S. Leonhardt, C. Ngo, et al., “Impedance-Controlled Variable Stiffness Actuator for Lower Limb Robot Applications”, *IEEE Trans. Automation Science and Engineering*, vol. 17, no. 2, pp.991-1004, Apr. 2020.
[29]. F. Ficuciell, L. Villan, and B. Siciliano, “Variable Impedance Control of Redundant Manipulators for Intuitive Human–Robot Physical Interaction”, *IEEE Trans. Robotics*, 2015, 31 (4): 850-863.
[30]. K. Kronander and A. Billard, “Stability Considerations for Variable Impedance Control”, *IEEE Trans. Robotics*, 2016, 32 (5): 1298-1305.
[31]. Y. Dong, and B. Ren, “UDE-Based Variable Impedance Control of Uncertain Robot Systems”, *IEEE Trans. Sys. Man and Syb.: Systems*, vol. 49, no. 12, pp.2487-2498, Dec. 2019.
[32]. F., C. Secchi, and C. Fantuzzi, “A tank-based approach to impedance control with variable stiffness,” in *Proc. IEEE Int. Conf. Robot. Autom.*, May 2013, pp. 4948–4953.
[33]. X. Liang, G. He, T. Su, et al, “Finite-Time Observer-Based Variable Impedance Control of Cable-Driven Continuum Manipulators”, *IEEE Trans. Human-Machine Systems*, vol. 52, no. 1, pp.26-40, Feb. 2022.
[34]. I. Ranatunga, F. L. Lewis, D. O. Popa, et al., “Adaptive Admittance Control for Human–Robot Interaction Using Model Reference Design and Adaptive Inverse Filtering”, *IEEE Trans. Cont. Sys. Tech.*, vol. 25, no. 1, pp.278-285, Jan. 2017.
[35]. Z. Feng, W. Liang, J. Ling, et al., “Adaptive Robust Impedance Control for an Ear Surgical Device With Soft Interaction”, *IEEE/ASME Trans. Mechatron.*, vol. 27, no. 3, pp. 1784-1795, Jun. 2022.
[36]. X. Yu, B. Li, W.He , et al., “Adaptive-Constrained Impedance Control for Human–Robot Co-Transportation”, *IEEE Trans. Cybernetics*,vol. 52, no. 12, pp., 13237-13249, Dec. 2022.
[37]. T. Qin, Y. Li, L. Quan, et al., “An Adaptive Robust Impedance Control Considering Energy-Saving of Hydraulic Excavator Boom and Stick Systems”, *IEEE/ASME Trans. Mechatron.*, vol. 27, no. 4, pp. 1928-1936, Aug. 2022.
[38]. E. Arefinia,H. A. Talebi, and A. Doustmohammadi, “A Robust Adaptive Model Reference Impedance Control of a Robotic Manipulator With Actuator Saturation”, *IEEE Trans. Sys. Man and Syb.: Systems*, vol. 50, no. 2, pp.409-420, Feb. 2020.
[39]. H. Huang, Y. Guo, G. Yang, et al., “Robust Passivity-Based Dynamical Systems for Compliant Motion Adaptation”, *IEEE/ASME Trans. Mechatron.*, vol. 27, no. 6, pp.4819-4828, Dec. 2022.
[40]. E. Arefifinia, H. A. Talebi, and A. Doustmohammadi, “A Robust Adaptive Model Reference Impedance Control of a Robotic Manipulator With Actuator Saturation”, *IEEE Trans. Sys. Man and Syb.: Systems*, vol. 50, no. 2, pp.409-420, Feb. 2020.
[41]. M. Sharifi, V. Azimi, V. K. Mushahwar, et al., “Impedance Learning-Based Adaptive Control for Human–Robot Interaction”, *IEEE Trans. Cont. Sys. Tech.*, vol. 30, no.4, pp.1345-1358, Jul. 2022.
[42]. Z. Li, X. Li, Q. Li, H. Su, Zh. Kan, and W. He, “Human-in-the-Loop Control of Soft Exosuits Using Impedance Learning on Different Terrains”, *IEEE Trans. Robotics*, vol. 38, no. 5, pp.2979-2993, Oct. 2022.
[43]. X. Yu, P. Liu, W. He, Y. Liu, Q. Chen, and L.Ding, “Human-Robot Variable Impedance Skills Transfer Learning Based on Dynamic Movement Primitives”, *IEEE Robotics and Automation Letter,* vol. 7, no. 3, pp. 6463-6470, Jul. 2022.
[44]. M. Sharififi, A.Zakerimanesh , J. K. Mehr, et al., “Impedance Variation and Learning Strategies in Human–Robot Interaction”, *IEEE Trans. Cybernetics,* vol. 52, no. 7, pp.6462-6475, Jul. 2022.
[45]. R. Wu and A. Billard, “Learning From Demonstration and Interactive Control of Variable-Impedance to Cut Soft Tissues”, *IEEE/ASME Trans. Mechatron.*, vol. 27, no. 5, pp.2740-2751, Oct.2022.
[46]. W. Zhang, L. Ott, M. Tognon, et al., “Learning Variable Impedance Control for Aerial Sliding on Uneven Heterogeneous Surfaces by Proprioceptive and Tactile Sensing,” *IEEE Robotics and Automation Letter,* vol. 7, no. 4, pp. 11275-11282, Oct. 2022.
[47]. M. Sharififi, V. Azimi, V. K. Mushahwar , et al., “Impedance Learning-Based Adaptive Control for Human–Robot Interaction”, *IEEE Trans. Cont. Sys. Tech.*, vol. 30, no. 4, pp. 1345-1358, Jul. 2022.
[48]. X. Xing, E. Burdet, W. Si, et al., “Impedance Learning for Human-Guided Robots in Contact With Unknown Environments”, *IEEE Trans. Robotics*, DOI:10.1109/TRO.2023.3281483.
[49]. Z. Li, J. Liu, Z. Huang, et al., “Adaptive Impedance Control of Human–Robot Cooperation Using Reinforcement Learning”, *IEEE Trans. Industrial Electronics*, vol.64, no.10, pp.8013-8022, Oct. 2017.
[50]. Z. Jin, D.Qin, A. Liu , et al., “Model Predictive Variable Impedance Control of Manipulators for Adaptive Precision-Compliance Tradeoff”, *IEEE/ASME Trans. Mechatron.*, vol. 28, no. 2, pp. 1174-1186, Apr. 2023.
[51]. X. Liu, S. S. Ge, F. Zhao, et al, “Optimized Impedance Adaptation of Robot Manipulator Interacting With Unknown Environment”, *IEEE Trans. Cont. Sys. Tech.*, vol. 29, no. 1, pp.411-419, Jan. 2021.
[52]. H. Wang, M. Tong, X. Zhao, et al, “ Predefined-Time Adaptive Neural Tracking Control of Switched Nonlinear Systems”, *IEEE Trans. Cybernetics,* DOI:10.1109/TCYB.2022. 3204275.
[53]. L. Liu, S. Leonhardt, and B. J. E. Misgeld, “Experimental Validation of a Torque-Controlled Variable Stiffness Actuator Tuned by Gain Scheduling”, *IEEE/ASME Trans. Mechatron.*, vol. 23, no. 5, pp.2109-2120, Oct. 2018.
[54]. H. Wang, K. Xu and H. Zhang, “Adaptive Finite-time Tracking Control of Nonlinear Systems with Dynamics Uncertainties”, *IEEE Trans. Automatic Control*, DOI 10.1109/TAC.2022.3226703.
[55]. X. Li, Y. Pan, G. Chen, and H. Yu, “Adaptive Human–Robot Interaction Control for Robots Driven by Series Elastic Actuators”, *IEEE Trans. Robotics*, vol. 33, no 1, pp.169-182, Feb. 2017.
[56]. Y.Huo, P.Li, D. Chen, et al, “Model-Free Adaptive Impedance Control for Autonomous Robotic Sanding”, *IEEE Trans. Automation Science and Engineering*, vol. 19, no.4, pp.3601-3611, Oct. 2022.
[57]. Y. Lin, Z. Chen, and B.Yao, “Unified Motion/Force/Impedance Control for Manipulators in Unknown Contact Environments Based on Robust Model-Reaching Approach”, *IEEE/ASME Trans. Mechatron.*, vol. 26, no. 4, Aug. 2021.
[58]. A. Astolfi, D. Karagiannis, and R. Ortega, *Nonlinear and Adaptive Control Design With Applications*. London, U.K.: Springer-Verlag, 2008.
[59]. I. Sarras, J.A. Acosta, R. Ortega, and A.D. Mahindrakar, “Constructive immersion and invariance stabilization for a class of under-actuated mechanical systems”, *Automatica*, vol.49, no.5, pp.1442–1448, 2013.
[60]. X.Dong, et al., "Continuum robots collaborate for safe manipulation of high-temperature flame to enable repairs in challenging environments." *IEEE/ASME Trans. Mechatron.*, vol.27, no.5, pp. 4217-4220, 2022.
[61]. N. Ma, et al., "Design and stiffness analysis of a class of 2-DoF tendon driven parallel kinematics mechanism." *Mechanism and Machine Theory* vol.129, pp.202-217,2018.
[62]. W. Ba, et al., "Design and validation of a novel fuzzy-logic-based static feedback controller for tendon-driven continuum robots." *IEEE/ASME Trans. Mechatron.*, vol. 26, no.6, pp.3010-3021, 2021.

Nan Ma received his Master and PhD degrees in North China University of Technology and Beihang University in 2015 and 2020, respectively. He worked at University of Nottingham of Mechanical Manufacturing and material Department from 2019 to 2021. From 2021, He works at Lancaster University of Engineering Department. His research interests are design, analysis, static and dynamic analysis of novel mechanisms for robots (e.g., parallel, continuum and soft robots), as well as design and fabrication.

David Cheneler received an MEng and a PhD in mechanical engineering from the University of Birmingham in 2005 and 2010 respectively. He was a research fellow at the University of Birmingham until joining Lancaster University as a Lecturer in 2013 before becoming a Senior Lecturer in 2020. His current research interests include the dynamics of robotic and mechatronic systems and nuclear engineering.

Guangping He (M'10) received the B.S., M.S., and Ph.D. degrees in mechanical and electrical engineering from the Beihang University of China, Beijing, China, in 1994, 1997, and 2002, respectively. During 1997 and 2002, he was with Launch Vehicle Technology Academy of China, Beijing. Since 2002, he has been with the Department of Mechanical and Electrical Engineering, North China University of Technology, Beijing. His current research interests include dynamics and control of robotic systems and micro-electromechanical devices.

Junjie Yuan received the B.S. and Ph.D. degrees in mechanical engineering from the Beijing Institute of Technology, Beijing, China, in 2001 and 2007, respectively. Since 2007, he has been with the Department of Mechanical and Electrical Engineering, North China University of Technology, Beijing. His current research interests include control of robotic system, as well as related sensor and mechatronics technology.

Gui-Bin Bian (M'15) received the Bachelor's degree in Mechanical Engineering from North China University of Technology, Beijing, China, in 2004, and the Master's and Doctoral degrees in Mechanical Engineering from Beijing Institute of Technology, Beijing, China, in 2007 and 2010 respectively.

He is a professor at the State Key Laboratory of Management and Control for Complex Systems, Institute of Automation, Chinese Academy of Sciences, Beijing, China, where his research interests include design, sensing and control for medical robotics.